Geochemical Perspectives Letters

High field strength elements in chondrites and their refractory components

C. Münker[1,2*], M. Pfeifer[1,2], V. Krisponeit[3], F. Wombacher[1]

OPEN ACCESS

https://doi.org/10.7185/geochemlet.2533

Abstract

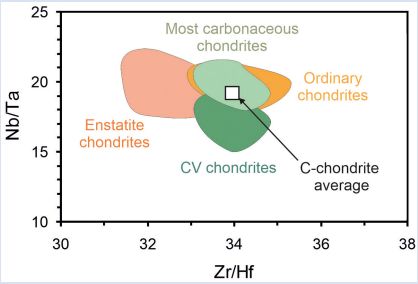

In geochemistry and cosmochemistry, chondrites provide important reference values for comparison with planetary compositions. Employing isotope dilution, we report a comprehensive high precision data set for the refractory high field strength elements (HFSEs; W-Nb-Ta-Zr-Hf) and Sm-Nd-Lu-U-Th in different types of chondrites and in refractory inclusions, mainly from CV3 chondrites. Except for U, parent body processes and terrestrial alteration appear to have negligible effects. The CI chondrite data allow calculation of canonical trace element ratios such as Nb/Ta, Zr/Nb, Zr/Hf, Hf/W or Th/U at unprecedented precision and accuracy. Enstatite chondrites exhibit resolvably lower Hf/W and Zr/Hf than carbonaceous and ordinary chondrites. Ratios of Nb/Ta are uniform between all chondrite classes and groups, except for CV chondrites, where Nb/Ta is lowered by admixture of refractory inclusions that display systematic depletions of the slightly less refractory and more siderophile Nb. Regarding parent-daughter ratios of the Lu-Hf, Sm-Nd, Hf-W, and Nb-Zr radioactive decay systems, the variations in chondrites and their refractory components must have already been established in the solar nebula by selective processing of metal and silicate components and condensation processes during CAI formation.

Received 8 January 2025 | Accepted 30 June 2025 | Published 10 September 2025

Introduction

In geochemistry and cosmochemistry, the extended group of high field strength elements (HFSEs; Nb, Ta, Zr, Hf and W which are all refractory and mostly lithophile) allows us to investigate processes related to condensation in the solar nebula and to planetary differentiation. Their abundances in chondritic meteorites provide an important reference composition for bulk planets and asteroids that is not affected by volatile element fractionation. During differentiation of planetary bodies, the two HFSEs W and, to a lesser extent, Nb may behave as siderophile or chalcophile and may be hosted by metal or sulfide phases (*e.g.*, Wade and Wood, 2001; Rubie *et al.*, 2011; Münker *et al.*, 2017). As all HFSEs have condensation temperatures above 1500 K (Lodders, 2003), they are traditionally seen as displaying little fractionation between different chondrite groups, with the notable exception of CV group carbonaceous chondrites (*e.g.*, Münker *et al.*, 2003; Kleine *et al.*, 2004). Recent work, however, suggested that some HFSE ratios like Nb/Ta, Zr/Nb or Hf/W might be fractionated between enstatite chondrites and other chondrite classes (Barrat *et al.*, 2014; Yoshizaki *et al.*, 2021; Hellmann *et al.*, 2024). The origin of these features has remained elusive but has been ascribed to early nebular heterogeneities caused by metal-silicate distribution, variable addition of refractory inclusions or redistribution on chondrite parent bodies (*e.g.*, Bouvier *et al.*, 2008; Barrat *et al.*, 2014). Likewise, HFSE patterns might also help to unravel the causes of the nucleosynthetic isotope dichotomy between non carbonaceous (CC) and carbonaceous (NCC) type chondrites (*e.g.*, Warren, 2011), which has previously been attributed to variable admixture of refractory materials (*e.g.*, Burkhardt *et al.*, 2019).

To better understand the HFSE inventory of chondrites and to update chondritic reference parameters, we determined the abundances of the HFSEs W, Nb, Ta, Zr, Hf and similarly incompatible and refractory elements (Th, U, Sm, Nd and Lu) in a comprehensive set of chondrites and some of their inclusions, including Ca, Al-rich inclusion (CAIs) with different refractory element depletion patters (type II and unfractionated) as well as amoeboid olivine aggregates (AOAs). All measurements were performed on the same meteorite split and at high precision, mostly employing isotope dilution and Multicollector ICPMS (MC-ICPMS). To compare the results with previous studies and to assess open system behaviour, our data set also includes radiogenic isotope data ($^{176}Hf/^{177}Hf$ and $^{143}Nd/^{144}Nd$) and for the inclusions also a complete set of rare earth elements (REE), obtained by solution quadrupole ICPMS on the same meteorite splits used for isotope dilution measurements. Notably, the chondrite samples analysed here include homogeneous powders prepared from comparatively large chondrite samples in previous studies, including the Orgueil CI chondrite (Barrat *et al.*, 2012), the Smithsonian Allende CV chondrite powder (Jarosewich *et al.*, 1987), as well as g-sized powder aliquots of enstatite chondrites (Braukmüller *et al.*, 2025). Such homogeneous samples are particularly suited to provide representative elemental abundances.

1. Institut für Geologie und Mineralogie, Universität zu Köln, Zülpicherstr. 49b, 50674 Köln, Germany
2. Steinmann Institut, Universität Bonn, Poppelsdorfer Schloss, 53115 Bonn, Germany
3. Geowissenschaftliches Zentrum, Universität Göttingen, Goldschmidtstr. 1-3, D-37077 Göttingen, Germany
* Corresponding author (Email: c.muenker@uni-koeln.de)

Sample Selection and Analytical Techniques

Details of the sample materials are given in the Supplementary Information. As for the carbonaceous and ordinary chondrites, we analysed splits prepared from <0.5 g-sized specimen (see also Münker *et al.*, 2003; Kleine *et al.*, 2004), but also powders that were prepared from 0.3–1.0 g-sized splits of the CI chondrites Orgueil ($n = 5$), Ivuna, and Alais, and one powder split of the CM chondrite Nogoya. For these eight powders, a comprehensive major and trace element data set was previously reported (Barrat *et al.*, 2012). The carbonaceous chondrite sample suite also includes different splits of the Allende USN reference powder (Jarosewich *et al.*, 1987), of which one split was previously analysed in Barrat *et al.* (2012) and the other split together with the Münster Allende powder (Münker *et al.*, 2003) was previously analysed by Braukmüller *et al.* (2018). We also prepared representative powders for 10 enstatite chondrites from 1–2 g-sized splits provided by NASA, analysed alongside with smaller splits prepared from *ca.* 0.5 g initial masses. Our compilation further includes complete chondrite data sets previously analysed in Münker *et al.* (2003) and Kleine *et al.* (2004), for which we now also report additional Lu and $^{176}Hf/^{177}Hf$ data for the same splits. To understand the anomalous HFSE distributions in CV chondrites, we also analysed aliquots of 12 CAIs and 4 AOAs from the CV chondrites Allende and NWA 2086 and the H6 chondrite NWA 7924. Data for CAI samples 1–6 were previously reported in Peters *et al.* (2017), for CAI samples 7–15 in Pfeifer (2017) and for A-33/44 in Jacobsen *et al.* (2008).

All isotope dilution measurements of HFSEs, U-Th and REEs were performed on the same chondrite split, using *ca.* 100 mg of powder prepared from the larger initial sample masses. Prior to digestion, these samples were spiked with mixed ^{183}W-^{180}Ta-^{180}Hf-^{176}Lu-^{94}Zr, ^{149}Sm-^{150}Nd and ^{229}Th-$^{233/236}U$ tracers that were calibrated against pure metal standards, identical to those used in the studies of Münker *et al.* (2003), Scherer *et al.* (2001) and Thiemens *et al.* (2019). Individual element cuts and a quantitative Zr/Nb fraction were separated by ion chromatography and measured by MC-ICPMS (protocols of Münker *et al.*, 2001; Weyer *et al.*, 2002; Thiemens *et al.*, 2019). The CV chondrite inclusions were first dissolved, and two liquid aliquots were (1) spiked for the measurements above, and (2) used for complementary trace element measurements by quadrupole ICPMS to classify the inclusions (see Supplementary Information).

Results and Discussion

Measured trace element and isotope data for the individual chondrite powders and CV chondrite inclusions (CAIs and AOAs) are given in the Supplementary Information. Chondrite data are plotted in Figure 1, average compositions for the different chondrite classes/groups are given in Table 1. Because of sample heterogeneity, powders prepared from smaller chondrite specimens (<0.5 g) appear to display larger scatter. However, most measured HFSE ratios (*i.e.* Zr/Nb, Zr/Hf, Lu/Hf) as well as present day and initial Hf-Nd isotope compositions overlap between most different chondrite classes and with previous high precision HFSE and Hf-Nd isotope studies on chondrites (*e.g.*, Weyer *et al.*, 2002; Münker *et al.*, 2003; Bouvier *et al.*, 2008; Stracke *et al.*, 2012). Enstatite chondrites and CV group carbonaceous chondrites are two notable exceptions for Nb/Ta (lower in CV chondrites and scattering in small (<1 g) enstatite chondrite splits) as well as Hf/W and Zr/Hf (lower in enstatite chondrites). The lower Nb/Ta in Allende and other CV chondrites were previously explained by a larger proportion

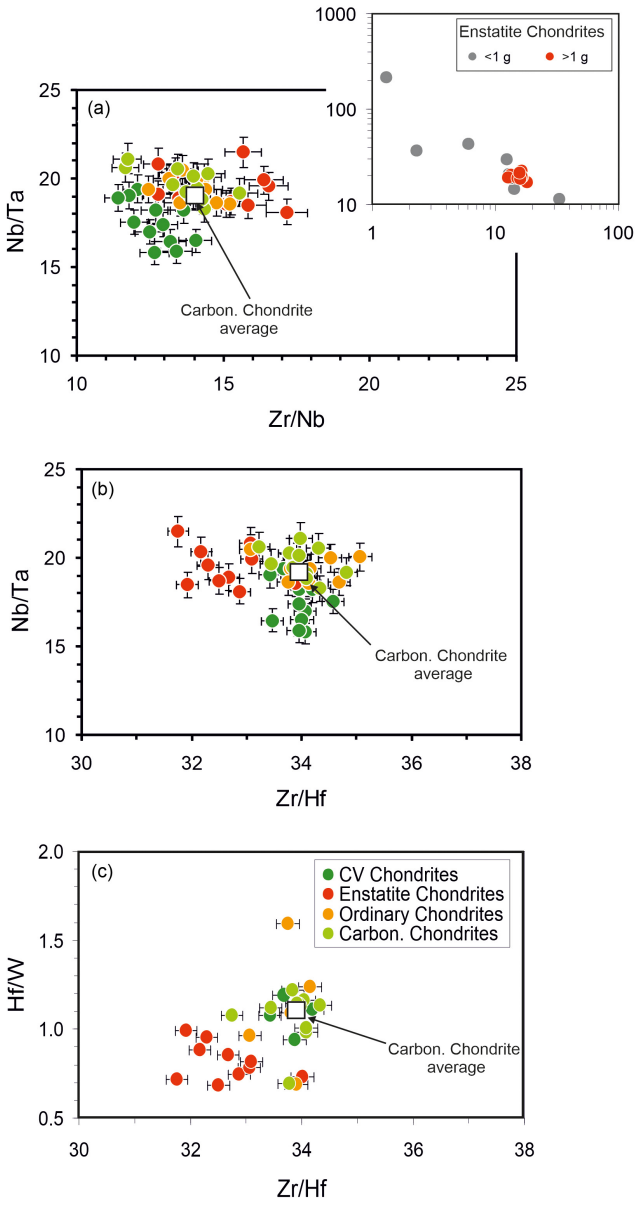

Figure 1 Plots of **(a)** Nb/Ta *versus* Zr/Nb, **(b)** Nb/Ta *versus* Zr/Hf and **(c)** Hf/W *versus* Zr/Hf, illustrating HFSE patterns in different chondrite classes and the CV group. The insert in **(a)** shows disturbed enstatite chondrite splits of low initial masses that exhibit a heterogeneous Nb distribution, resulting in fractionated Nb/Ta. CV group chondrites display resolvably lower Nb/Ta and enstatite chondrites lower Zr/Hf and Hf/W than all other classes/groups. The carbonaceous chondrite average shown excludes CV chondrites.

of ultra-refractory material with low Nb/Ta (*e.g.*, Stracke *et al.*, 2012; Münker *et al.*, 2017), which can now be confirmed by the consistently lower Nb/Ta in CAIs (3.3–18.3), whereas AOAs display both lower and higher values (4.1–24).

As closest analogues to the bulk solar system composition, the CI chondrite powders of Orgueil, Ivuna and Alais (*cf.* Barrat *et al.*, 2012) display average W, Zr, Hf and Ta contents of 95.6 ng/g, 3.62 µg/g, 107 ng/g and 13.7 ng/g, respectively, in good agreement with the CI chondrite estimates by Palme and O'Neill (2014), but markedly lower than reported by earlier high precision studies (Münker *et al.*, 2003; Kleine *et al.*, 2004), where many smaller meteorite splits in the 0.1–0.2 g range were analysed. Corresponding Nb/Ta, Zr/Nb, Zr/Hf and Hf/W for CI chondrites are 19.0 ± 0.4, 14.0 ± 0 .8, 33.9 ± 0.5 and 1.12 ± 0.07

Table 1 Average HFSE abundances and element ratios as well as radiogenic isotope compositions measured for different chondrite classes and groups. We recommend the CI averages to be used as canonical ratios in geochemical and cosmochemical studies. Except for CV chondrites (not shown, see Table S-1) and some enstatite chondrites (see Table S-2), Nb/Ta, Zr/Nb and Lu/Hf overlap between all chondrite classes and groups. Ratios of Hf/W and Zr/Hf in enstatite chondrites are resolvably lower. Note that 95 % c.i. errors include Student's *t* factors.

	Orgueil Powders			CI (Orgueil, Ivuna, Alais)			Enstatite chondrites			Ordinary chondrites		
	Mean	2 s.d.	95 % c.i.	Mean	2 s.d.	95 % c.i.	Mean	2 s.d.	95 % c.i.	Mean	2 s.d.	95 % c.i.
µg/g												
Zr	3.66	0.08	0.05	3.62	0.18	0.08	3.94	1.04	0.35	5.27	0.73	0.23
Nb	0.257	0.022	0.014	0.259	0.025	0.012	0.254	0.109	0.036	0.384	0.056	0.020
Ta	0.0138	0.0003	0.0002	0.0137	0.0005	0.0002	0.0134	0.0058	0.0019	0.0193	0.0041	0.0015
Sm	0.140	0.009	0.006	0.144	0.021	0.010	0.165	0.075	0.027	0.172	0.073	0.023
Nd	0.432	0.026	0.016	0.443	0.061	0.028	0.484	0.185	0.066	0.531	0.230	0.073
Lu	0.0254	0.0024	0.0015	0.0255	0.0020	0.0009	0.0288	0.0098	0.0033	0.0322	0.0080	0.0025
Hf	0.108	0.003	0.002	0.107	0.004	0.002	0.121	0.030	0.010	0.154	0.020	0.006
W	0.0931	0.0039	0.0024	0.0956	0.0101	0.0047	0.151	0.058	0.020	0.145	0.074	0.046
Th	0.0279	0.0010	0.0006	0.0283	0.0021	0.0010	0.0344	0.0165	0.0055	-	-	-
U	0.00766	0.00062	0.00038	0.00874	0.00392	0.00182	0.0108	0.0108	0.0036	-	-	-
$^{176}Lu/^{177}Hf$	0.0335	0.0024	0.0015	0.0339	0.0024	0.0011	0.0339	0.0071	0.0024	0.0299	0.0085	0.0027
$^{176}Hf/^{177}Hf$	0.282875	0.000221	0.000138	0.282902	0.000203	0.000094	0.282896	0.000738	0.000248	0.282550	0.000744	0.000236
εHf(0)	3.6	7.8	4.9	4.6	7.2	3.3	4.4	26.1	8.8	-7.9	26.3	8.4
εHf(4565)	2.7	1.3	0.8	2.4	1.6	0.7	2.2	6.1	2.1	2.6	2.3	0.7
$^{147}Sm/^{144}Nd$	0.1959	0.0013	0.0008	0.1961	0.0016	0.0008	0.1964	0.0062	0.0022	0.1956	0.0034	0.0021
$^{143}Nd/^{144}Nd$	0.512651	0.000057	0.000035	0.512654	0.000052	0.000024	0.512777	0.000114	0.000041	0.512667	0.000183	0.000114
εNd(now)	0.3	1.1	0.7	0.3	1.0	0.5	2.7	2.2	0.8	0.6	3.6	2.2
εNd(4565)	0.8	0.4	0.3	0.7	0.5	0.2	2.9	2.4	0.8	1.2	1.9	1.2
Nb/Ta	19.0	1.0	0.7	19.0	0.9	0.4	19.0	2.6	0.9	19.5	1.4	0.5
Zr/Hf	34.0	0.4	0.2	33.9	1.0	0.5	32.7	1.5	0.5	34.2	1.1	0.3
Zr/Nb	14.3	1.3	0.8	14.0	1.7	0.8	15.8	3.3	1.1	13.8	1.8	0.6
Hf/W	1.16	0.08	0.05	1.12	0.15	0.07	0.82	0.30	0.10	1.12	0.67	0.42
$^{180}Hf/^{184}W$	1.36	0.09	0.06	1.32	0.17	0.08	0.97	0.36	0.12	1.32	0.79	0.49
Hf/Ta	7.83	0.40	0.25	7.49	1.70	0.79	9.15	1.90	0.64	7.95	0.97	0.35
W/Th	3.34	0.24	0.15	3.38	0.38	0.18	4.53	2.28	0.77	-	-	-
W/U	12.2	1.4	0.9	11.3	3.4	1.6	15.8	10.8	3.6	-	-	-
Th/U	3.64	0.16	0.10	3.34	1.10	0.51	3.49	1.59	0.53	-	-	-

(corresponding to $^{180}Hf/^{184}W = 1.32$; all errors 95 % c.i.). Measured element ratios for CM and CK chondrites as well as for ordinary chondrites overlap within error with CI chondrites (Figs. 1, S-2), although absolute element abundances can be substantially higher. The Orgueil splits yield an average Th/U of 3.64 ± 0.10, while Alais and Ivuna deviate towards lower values, likely due to secondary U enrichment (10.5 and 12.5 ng/g U compared to 7.7 ± 0.4 ng/g U in Orgueil). Collectively, we therefore propose to use the CI chondrite averages as canonical solar system values for the HFSE W-Nb-Ta-Zr-Hf-Lu, whereas due to apparent U mobility in the Alais and Ivuna splits analysed we propose to only use the Orgueil average as canonical value for Th/U.

While Zr/Hf and Hf/W in enstatite chondrites (32.7 ± 0.5 and 0.82 ± 0.10, respectively) are slightly lower than in other classes, Nb/Ta ratios display a vast scatter, ranging from 11.3–213, with extreme scatter displayed by samples with smallest masses of initially prepared powders. As Nb/Ta varies with Zr/Nb and Nb abundances (inset in Fig. 1a), but not with other parameters, we conclude that the scatter is caused by selective re-distribution of Nb into metal or sulfide phases, confirming earlier findings (*e.g.*, Barrat *et al.*, 2014). Notably, except for W, Nb is the HFSE with the strongest siderophile-chalcophile affinities at more reduced conditions (*e.g.*, Wade and Wood, 2001; Münker *et al.*, 2017). As no positive correlation between Zr/Nb and Hf/W has been found between different classes and EL-EH groups (Fig. S-2), nebular processes are the most likely cause for the lower Hf/W in enstatite chondrites. When limited to a subset of larger initial sample mass (>1 g), Zr/Nb in the enstatite chondrites is approaching more unfractionated values, and an average Nb/Ta of 19.0 ± 0.9 (95 % c.i.) is calculated. This value is indistinguishable from the CI average, but inconsistent with previous work claiming a different average Nb/Ta for the enstatite chondrite reservoir (Yoshizaki *et al.*, 2021).

The high precision HFSE data obtained for CAIs and AOAs allow valuable insights into the mechanisms controlling the HFSE budget of chondrites (Fig. 2). Compared to chondrites, type II CAIs are markedly depleted in highly refractory elements such as Lu, Zr and Hf relative to Ta and Nb, and show correspondingly lower Zr/Nb (Table S-4), as they condensed from nebular reservoirs previously depleted in these highly refractory elements (*e.g.*, Kornacki and Fegley, 1986). As a second competing process, Nb is always variably depleted relative to Ta, leading to overall lower Nb/Ta. This may be seen in the light of a slightly more volatile behaviour of Nb predicted from thermodynamic data (*e.g.*, Lodders, 2003) but may also reflect more siderophile properties of Nb at the more reducing conditions prevailing during CAI formation. CAIs with unfractionated REE patterns

("unfractionated" group in Fig. S-1; *e.g.*, type III) display little variation in Lu-Zr-Hf, but are again variably depleted in Nb. Model calculations in Figure 2 show that admixture of 2–5 % type II or type III CAIs with their uniformly low Nb/Ta can explain the lower Nb/Ta measured in CV chondrites, in line with previous studies (*e.g.*, Stracke *et al.*, 2012; Alexander *et al.*, 2019). With the exception of Zr-Hf, type II CAIs dominate the element budget of HFSE and REE (Fig. 2). Notably, effects on other HFSE ratios such as Zr/Hf or Lu/Hf are negligible, because Zr/Hf is only fractionated in type II CAIs with their extremely low Zr-Hf-Lu contents that insignificantly contribute to the bulk chondrite budget. Conversely, Zr/Hf or Lu/Hf are not fractionated in unfractionated CAIs that are not depleted in these elements and contribute to the chondrite budget to a larger extent. As in chondrites, refractory inclusions exhibit a somewhat larger range of Th/U (0.58–9.34), which in the light of similarly high condensation temperatures (Lodders, 2003) and the lack of a consistent depletion or enrichment pattern, we ascribe to alteration on the parent bodies or terrestrial alteration.

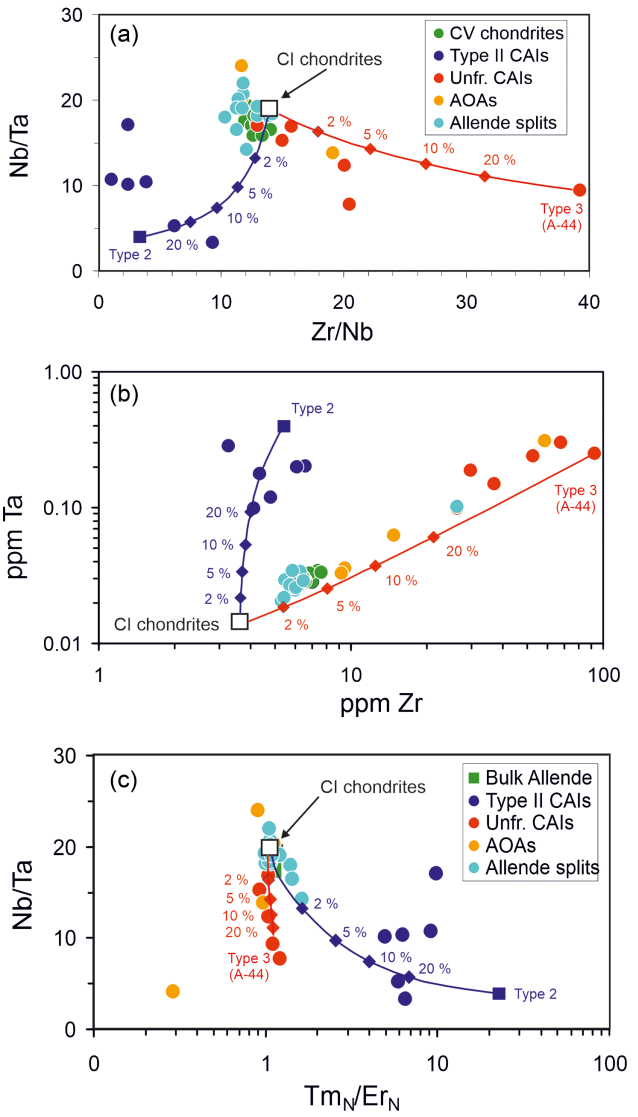

Figure 2 Plots illustrating the effect of refractory inclusions (CAIs and AOAs) on the HFSE inventory of CV chondrites. **(a)** Nb/Ta *vs.* Zr/Nb, **(b)** Zr *vs.* Ta and **(c)** Nb/Ta *vs.* Tm_N/Er_N. The plots also include previously published high precision HFSE data for small Allende fractions (Stracke *et al.*, 2012). Mixing lines illustrate that the distinct Nb depletions in CV chondrites result from the addition of variable proportions of both type II and unfractionated refractory material (type II CAI after Stracke *et al.*, 2012 and A-44 as unfractionated type III CAI were used as end members).

Based on nucleosynthetic isotope anomalies, Burkhardt *et al.* (2019) argued that variable admixture of CAIs can explain the full compositional array from non-carbonaceous chondrites (NCCs) to carbonaceous chondrites (CCs), with CV chondrites as the most CAI-rich end member. While our HFSE data can confirm their conclusions for the carbonaceous chondrites, the difference between NCCs to CCs is difficult to explain. In this case NCCs should display resolvably higher Nb/Ta ratios than CCs, which, in contrast to CV chondrites, is not observed. The same conclusion derives from Hf/W (Fig. 3), which is lower in type II CAIs due to depletion of Hf. Admixture of type II CAIs would therefore lower Hf/W but, rather, Hf/W is lowest in the enstatite chondrites, contrary to the prediction from nucleosynthetic isotope anomalies. Likewise, combined ^{50}Ti-^{54}Cr-^{62}Ni nucleosynthetic isotope patterns in chondrites cannot be reproduced by simple mixing with refractory components only (Palme and Mezger, 2024). The systematically lower Hf/W found for enstatite chondrites agree with inferences from ^{182}Hf-^{182}W relationships (Hellmann *et al.*, 2024), where the difference was attributed (1) to addition of CAIs, or (2) to chondrule formation processes. Based on HFSE systematics reported here (indistinguishable Nb/Ta), their first model can now be ruled out (even for type II CAIs), making Hf-W fractionation in the early solar nebula related to chondrule formation the most plausible explanation. Furthermore, metal or sulfide segregation can be excluded, as Zr/Nb and Hf/W lack a positive correlation (Fig. S-2).

Figure 3 illustrates the effects of refractory inclusions on parent-daughter ratios of short (^{182}Hf-^{182}W, ^{92}Nb-^{92}Zr) and long lived (^{176}Lu/^{177}Hf, ^{147}Sm-^{143}Nd) radioactive decay systems in chondrites and their components. Here, parent-daughter ratios are plotted *versus* Tm_N/Er_N as measure of refractory element fractionation at high temperatures. In most cases, the element ratios are either constant or vary systematically with Tm_N/Er_N, illustrating that secondary redistribution during parent body alteration is rather insignificant at the sample scale. For the two long lived decay systems discussed here, effects of refractory inclusions are negligible, because all groups of inclusions overlap in their Sm/Nd and Lu/Hf with those of bulk chondrites (Fig. 3a,d). If mineral scale redistribution on parent bodies by secondary processes (*e.g.*, for Lu by crystallisation of phosphates; *e.g.*, Bouvier *et al.*, 2008) is neglected, most chondrites therefore show uniform parent-daughter ratios for Lu/Hf and Sm/Nd, irrespective of their petrological type and CAI contents. For the ^{92}Nb-^{92}Zr system, the effects depend on the type of inclusion. Type II CAIs with their extremely depleted Zr contents will lower Zr/Nb, whereas unfractionated CAIs with their higher Zr/Nb and depleted Nb will increase Zr/Nb without concomitant fractionation of Tm/Er (Fig. 3c). This particularly explains the somewhat larger than analytical scatter in Zr/Nb (Fig. 1a) that is even observed within individual groups of carbonaceous chondrites that otherwise display much more homogenous HFSE ratios. In contrast to the carbonaceous chondrites, the secondary redistribution of Zr/Nb in some enstatite chondrites at smaller sample scales (insert in Fig. 1a) is linked to the chalcophile behaviour of Nb (Barrat *et al.*, 2014 and leaching experiments therein). Systematics of Hf and W in the inclusions (Fig. 3b) show similar patterns as for Zr/Nb. Here, unfractionated CAIs (and most types of AOAs) will not affect Hf/W or only cause a slight increase. Conversely, addition of type II CAIs causes a decrease of Hf/W, but this might not be resolvable, as they display low contents of Hf. Most importantly, type II inclusions cannot account for the lower Hf/W of the enstatite chondrite class (Table 1), because this would be accompanied by a marked decrease in Nb/Ta which is not observed (Fig. 1).

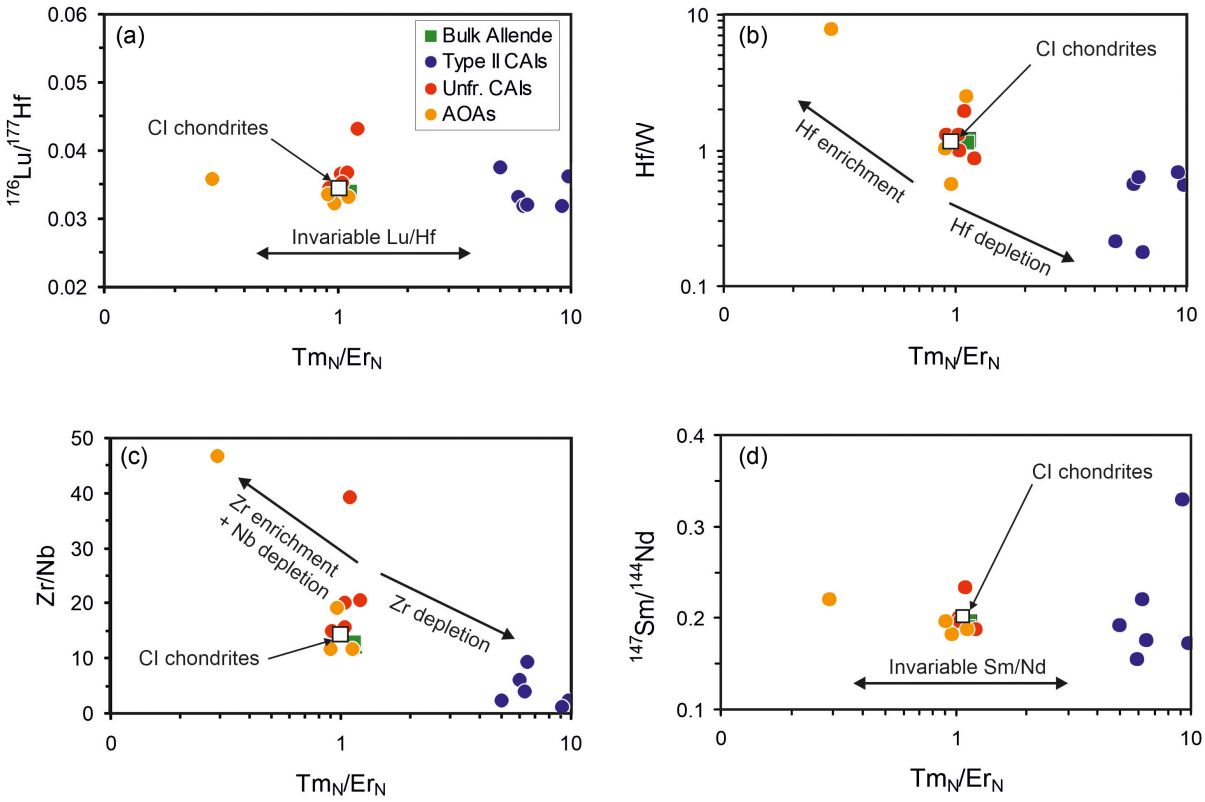

Figure 3 Plots illustrating the effect of CAIs on parent-daughter ratios of important long and short lived decay systems, where Tm_N/Er_N traces different types of refractory inclusions with different volatile depletion trends.

Hence, the low Hf/W of the enstatite chondrite group is rather an intrinsic feature of the inner solar system region. Collectively, the HFSE parent-daughter fractionations found in chondrites and their components likely mirror compositional gradients in the solar nebular before parent body formation.

Conclusions

New high precision measurements of HFSEs together with U/Th, Lu/Hf, and Sm/Nd ratios, all obtained by isotope dilution, provide more accurate chondritic reference values for these elements which are important anchors in planetary evolution studies. Collectively, HFSE compositions of chondritic meteorites from different regions of the solar system illustrate an overall solar system homogeneity for refractory HFSE (Zr, Hf, Ta), REE (Nd-Sm-Lu) and U-Th. The addition of refractory inclusions to carbonaceous chondrites of the CV group resulted in selective depletions of the slightly less refractory Nb compared to other refractory elements. Niobium also partitions into sulfides in reduced enstatite chondrites, resulting in small scale heterogeneities. Chondrites from the inner solar system exhibit resolvably lower Hf/W and Zr/Hf than those from outer regions. Parent-daughter ratios of long and short lived isotope systems studied here are uniform for Sm/Nd and Lu/Hf across chondrite-forming reservoirs. For Nb-Zr and Hf-W, the strong fractionation effects observed for inclusions and to a lesser extent for bulk chondrites originate from early processes in the solar nebula. Parent body effects are identified for Lu/Hf in ordinary chondrites and Zr/Nb in enstatite chondrites, where secondary phosphates and metals/sulfides, respectively, caused redistribution of Lu and Nb. Importantly, HFSE patterns in chondrites are inconsistent with models claiming that variable admixture of refractory material can explain the full compositional array from non-carbonaceous to carbonaceous chondrites.

Acknowledgements

This paper was written during a sabbatical stay of CM at the University of Florence and CNR Pisa, Italy. We thank Jean-Alix Barrat and Andreas Pack for discussion and providing samples. Antarctic chondrite samples were generously provided by NASA, others by Jutta Zipfel, Senckenberg Museum, Frankfurt, Addi Bischoff, Universität Münster, Renate Schumacher, Mineralogisches Museum, Universität Bonn, Stefan Peters, Mineralogische Sammlung LIB Hamburg, and by the Smithsonian Museum, Washington. CM acknowledges funding through the European Commission by ERC grant 669666 "Infant Earth" and by the DFG through SPP 1833 "Habitable Earth". VK acknowledges funding through DFG grants Pa 909/7-1/2. Constructive reviews by Kathryn Shaw and Tetsuya Yokoyama as well as by editor Helen Williams helped to improve the manuscript.

Editor: Helen Williams

Additional Information

Supplementary Information accompanies this letter at https://www.geochemicalperspectivesletters.org/article2533.

Cite this letter as: Münker, C., Pfeifer, M., Krisponeit, V., Wombacher, F. (2025) High field strength elements in chondrites and their refractory components. *Geochem. Persp. Let.* 36, 42–47. https://doi.org/10.7185/geochemlet.2533

References

Alexander, C.M.O'D. (2019) Quantitative models for the elemental and isotopic fractionations in chondrites: The carbonaceous chondrites. *Geochimica et Cosmochimica Acta* 254, 277–309. https://doi.org/10.1016/j.gca.2019.02.008

Barrat, J.A., Zanda, B., Moynier, F., Bollinger, C., Liorzou, C., Bayon, G. (2012) Geochemistry of CI chondrites: Major and trace elements, and Cu and Zn Isotopes. *Geochimica et Cosmochimica Acta* 83, 79–92. https://doi.org/10.1016/j.gca.2011.12.011

Barrat, J.A., Zanda, B., Jambon, A., Bollinger, C. (2014) The lithophile trace elements in enstatite chondrites. *Geochimica et Cosmochimica Acta* 128, 71–94. https://doi.org/10.1016/j.gca.2013.11.042

Bouvier, A., Vervoort, J.D., Patchett, P.J. (2008) The Lu–Hf and Sm–Nd isotopic composition of CHUR: Constraints from unequilibrated chondrites and implications for the bulk composition of terrestrial planets. *Earth and Planetary Science Letters* 273, 48–57. https://doi.org/10.1016/j.epsl.2008.06.010

Braukmüller, N., Wombacher, F., Hezel, D.C., Escoube, R., Münker, C. (2018) The chemical composition of carbonaceous chondrites: Implications for volatile element depletion, complementarity and alteration. *Geochimica et Cosmochimica Acta* 239, 17–48. https://doi.org/10.1016/j.gca.2018.07.023

Braukmüller, N., Funk, C., Abouchami, W., Pickard, H., Rehkämper, M., Bragagni, A., Galer, S.J.G., Münker, C., Becker, H., Wombacher, F. (2025) Moderately volatile elements in chondrites record chondrule formation, two-component mixing and redistribution on parent bodies. *Geochimica et Cosmochimica Acta* 393, 43–62. https://doi.org/10.1016/j.gca.2025.02.001

Burkhardt, C., Dauphas, N., Hans, U., Bourdon, B., Kleine, T. (2019) Elemental and isotopic variability in solar system materials by mixing and processing of primordial disk reservoirs. *Geochimica et Cosmochimica Acta* 261, 145–170. https://doi.org/10.1016/j.gca.2019.07.003

Hellmann, J.L., Van Orman, J.A., Kleine, T. (2024) Hf-W isotope systematics of enstatite chondrites: Parent body chronology and origin of Hf-W fractionations among chondritic meteorites. *Earth and Planetary Science Letters* 626, 118518. https://doi.org/10.1016/j.epsl.2023.118518

Jacobsen, B., Yin, Q.-z., Moynier, F., Amelin, Y., Krot, A.N., Nagashima, K., Hutcheon, I.D., Palme, H. (2008) ^{26}Al–^{26}Mg and ^{207}Pb–^{206}Pb systematics of Allende CAIs: Canonical solar initial ^{26}Al/^{27}Al ratio reinstated. *Earth and Planetary Science Letters* 272, 353–364. https://doi.org/10.1016/j.epsl.2008.05.003

Jarosewich, E., Clarke Jr., R.S., Barrows, J.N. (1987) *Allende Meteorite Reference Sample*. Smithsonian Contributions to the Earth Sciences, Washington, D.C., 27, 1–49. https://doi.org/10.5479/si.00810274.27.1

Kleine, T., Mezger, K., Münker, C., Palme, H., Bischoff, A. (2004) ^{182}Hf-^{182}W isotope systematics of chondrites, eucrites, and martian meteorites: Chronology of core formation and early mantle differentiation in Vesta and Mars. *Geochimica et Cosmochimica Acta* 68, 2935–2946. https://doi.org/10.1016/j.gca.2004.01.009

Kornacki, A.S., Fegley Jr., B. (1986) The abundance and relative volatility of refractory trace elements in Allende Ca, Al-rich inclusions: implications for chemical and physical processes in the solar nebula. *Earth and Planetary Science Letters* 79, 217–234. https://doi.org/10.1016/0012-821X(86)90180-9

Lodders, K. (2003) Solar System Abundances and Condensation Temperatures of the Elements. *The Astrophysical Journal* 591, 1220–1247. https://doi.org/10.1086/375492

Münker, C., Weyer, S., Scherer, E., Mezger, K. (2001) Separation of high field strength elements (Nb, Ta, Zr, Hf) and Lu from rock samples for MC-ICPMS measurements. *Geochemistry, Geophysics, Geosystems* 2, 2001GC000183. https://doi.org/10.1029/2001GC000183

Münker, C., Pfänder, J.A., Weyer, S., Büchl, A., Kleine, T., Mezger, K. (2003) Evolution of Planetary Cores and the Earth-Moon System from Nb/Ta Systematics. *Science* 301, 84–87. https://doi.org/10.1126/science.1084662

Münker, C., Fonseca, R.O.C., Schulz, T. (2017) Silicate Earth's missing niobium may have been sequestered into asteroidal cores. *Nature Geoscience* 10, 822–826. https://doi.org/10.1038/ngeo3048

Palme, H., Mezger, K. (2024) Nucleosynthetic isotope variations in chondritic meteorites and their relationship to bulk chemistry. *Meteoritics and Planetary Science* 59, 382–394. https://doi.org/10.1111/maps.14127

Palme, H., O'Neill, H.St.C. (2014) 3.1 - Cosmochemical Estimates of Mantle Composition. In: Holland, H.D., Turekian, K.K. (Eds.) *Treatise on Geochemistry*. Elsevier, Amsterdam, 1–39. https://doi.org/10.1016/B978-0-08-095975-7.00201-1

Peters, S.T.M., Münker, C., Pfeifer, M., Elfers, B.-M., Sprung, P. (2017) Distribution of p-process ^{174}Hf in early solar system materials and the origin of nucleosynthetic Hf and W isotope anomalies in Ca–Al rich inclusions. *Earth and Planetary Science Letters* 459, 70–79. https://doi.org/10.1016/j.epsl.2016.11.009

Pfeifer, M. (2017) *The Tantalum isotope inventory of terrestrial and early solar system materials*. PhD thesis, University of Cologne, Germany. http://kups.ub.uni-koeln.de/id/eprint/7881.

Rubie, D.C., Frost, D.J., Mann, U., Asahara, Y., Nimmo, F., Tsuno, K., Kegler, P., Holzheid, A., Palme, H. (2011) Heterogeneous accretion, composition and core–mantle differentiation of the Earth. *Earth and Planetary Science Letters* 301, 31–42. https://doi.org/10.1016/j.epsl.2010.11.030

Scherer, E., Münker, C., Mezger, K. (2001) Calibration of the Lutetium-Hafnium Clock. *Science* 293, 683–687. https://doi.org/10.1126/science.1061372

Stracke, A., Palme, H., Gellissen, M., Münker, C., Kleine, T., Birbaum, K., Günther, D., Bourdon, B., Zipfel, J. (2012) Refractory element fractionation in the Allende meteorite: Implications for solar nebula condensation and the chondritic composition of planetary bodies. *Geochimica et Cosmochimica Acta* 85, 114–141. https://doi.org/10.1016/j.gca.2012.02.006

Thiemens, M.M., Sprung, P., Fonseca, R.O.C., Leitzke, F.P., Münker, C. (2019) Early Moon formation inferred from hafnium–tungsten systematics. *Nature Geoscience* 12, 696–700. https://doi.org/10.1038/s41561-019-0398-3

Wade, J., Wood, B.J. (2001) The Earth's 'missing' niobium may be in the core. *Nature* 409, 75–78. https://doi.org/10.1038/35051064

Warren, P.H. (2011) Stable-isotopic anomalies and the accretionary assemblage of the Earth and Mars: A subordinate role for carbonaceous chondrites. *Earth and Planetary Science Letters* 311, 93–100. https://doi.org/10.1016/j.epsl.2011.08.047

Weyer, S., Münker, C., Rehkämper, M., Mezger, K. (2002) Determination of ultra-low Nb, Ta, Zr and Hf concentrations and the chondritic Zr/Hf and Nb/Ta ratios by isotope dilution analyses with multiple collector ICP-MS. *Chemical Geology* 187, 295–313. https://doi.org/10.1016/S0009-2541(02)00129-8

Yoshizaki, T., Ash, R.D., Lipella, M.D., Yokoyama, T., McDonough, W.F. (2021) Variable refractory lithophile element compositions of planetary building blocks: Insights from components of enstatite chondrites. *Geochimica et Cosmochimica Acta* 308, 173–187. https://doi.org/10.1016/j.gca.2021.05.057